Target Detection using Weather Radars and Electromagnetic Vector Sensors

Prateek Gundannavar and Arye Nehorai

Email: nehorai@ese.wustl.edu

Preston M. Green Department of Electrical & Systems Engineering
Washington University in St. Louis

August 23, 2017

Acknowledgement

- Dr. Martin Hurtado
  - Department of Electrical Engineering, National University of La Plata, La Plata 1900, Argentina.

- AFOSR grants
  - FA9550-11-1-0210
  - FA9550-16-1-0386

Outline

- Passive radar
- Signal model and statistics
- Generalized likelihood ratio test detector
- Numerical results
- Future work

Outline

- Passive radar
- Signal model and statistics
- Generalized likelihood ratio test detector
- Numerical results
- Future work

Passive Radar: Introduction

- Improving the detection performance of a target can be important for military and surveillance operations.
- A radar network consisting of non-cooperative illuminators of opportunity (IO) and one or several passive receivers is referred to as a passive radar network.
- Non-cooperative IO include:
  - FM radio waves
  - Television and audio broadcast signals
  - Satellite and mobile communication based signals
  - Weather radar electromagnetic waves

Passive Radar: Advantages and Challenges

Advantages:

- Smaller, lighter, and cheaper over active radars
- Less prone to jamming
- Resilience to anti-radiation missiles
- Stealth operations
- ...

Challenges:

- Rely on third-party illuminators
- Waveforms out of control which leads to poor spatial/doppler resolution
- ...

Passive Bistatic Radar: Geometry of EMVS Receiver

- The signal arriving at the receiver consists of the signal from the non-cooperative transmitter (transmitter-to-receiver), which is referred to as the reference path, and the echoes generated by the reflection of the transmitted signal from the target (target-to-receiver), which are referred to as the surveillance path.

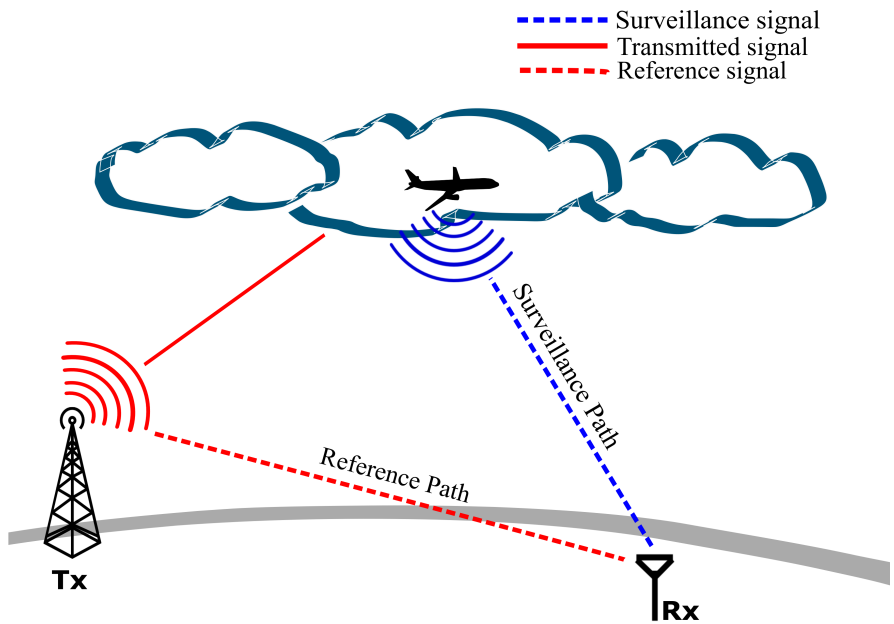

Figure 1: Spatial and temporal filtering techniques isolate the reference from the surveillance channel.

Passive Radar: Existing Methods

Cross ambiguity function (CAF):

- The transmitted signal is estimated from the reference channel, and cross-correlated with the signal in the surveillance channel. The resulting function called the cross-ambiguity function which mimics a matched filter output, and is given as

$$\chi(\eta,\nu) = \int_{-\infty}^{+\infty} y_{\mathrm{s}}(t) y_{\mathrm{r}}^{*}(t-\eta) e^{j2\pi\nu t} dt, \tag{1}$$

  where $y_{\mathrm{s}}(t)$ and $y_{\mathrm{r}}(t)$ are the surveillance and refernece channel received signals, and η and ν represents the target delay and Doppler, respectively.

Generalized likelihood ratio test (GLRT):

- Only the surveillance channel is considered, due to which the detector does not require knowledge of the transmitter position or the reference channel signal-to-noise ratio (SNR).

Passive Radar: Drawbacks

Cross ambiguity function (CAF):

- When a good estimate of the reference channel signal is not available, which occurs due to propagation losses, presence of clutter, and blockage or non-availability of the line-of-sight, the performance of the CAF-based detector decreases.

Generalized likelihood ratio test (GLRT):

- The existing GLRT-based methods do not consider the effect of clutter in the surveillance path.
- For continuous IOs such as DVB-T transmitters, signal-dependent clutter may arise due to multipath reflections of the surveillance signal. For weather surveillance radars, signal-dependent clutter occurs due to the hydrometeors present in the range gate of interest.

Weather Radar as Illuminator of Opportunity: Motivation

Coverage area:

- There are 150 nearly identical dual-polarized S-band Doppler weather surveillance radars in the USA, with an observation range of $230 - 460\,\mathrm{km}$ and a range resolution of $0.25 - 1\,\mathrm{km}$, depending on the mode of operation.

Modeling:

- Lack of statistical signal model that considers signal-dependent clutter model for target detection with weather surveillance radar as IO.

Polarized receivers:

- Exploiting the polarimetric information about the target with the help of diversely polarized antennas such as electromagnetic vector sensors (EMVS).

Passive Radar: Our Contributions

- We propose a passive bistatic network, with weather surveillance radar as the IO and electromagnetic vector sensor (EMVS) as the receiver. To the best of our knowledge, no previous work on passive bistatic radar addressed employing a weather radar for target detection.

- We believe we are the first to consider polarization information for mitigating signal-dependent clutter and improve detection in a passive radar, with weather surveillance radar as IO.

- We propose a maximum likelihood (ML) solution to extract the signal subspace from the received data contaminated by the clutter interference. We also propose a generalized likelihood ratio test (GLRT) detector that is robust to inhomogeneous clutter.

- We provide the exact distribution of the test statistic for the asymptotic case and evaluate its performance loss by considering a reduced set of data.

Outline

- Passive radar
- Signal model and statistics
- Generalized likelihood ratio test detector
- Numerical results
- Future work

Problem Description: Bistatic Passive Polarimetric Radar

Goal: Target detection in a bistatic passive polarimetric radar network, with weather surveillance radar as our illuminator of opportunity.

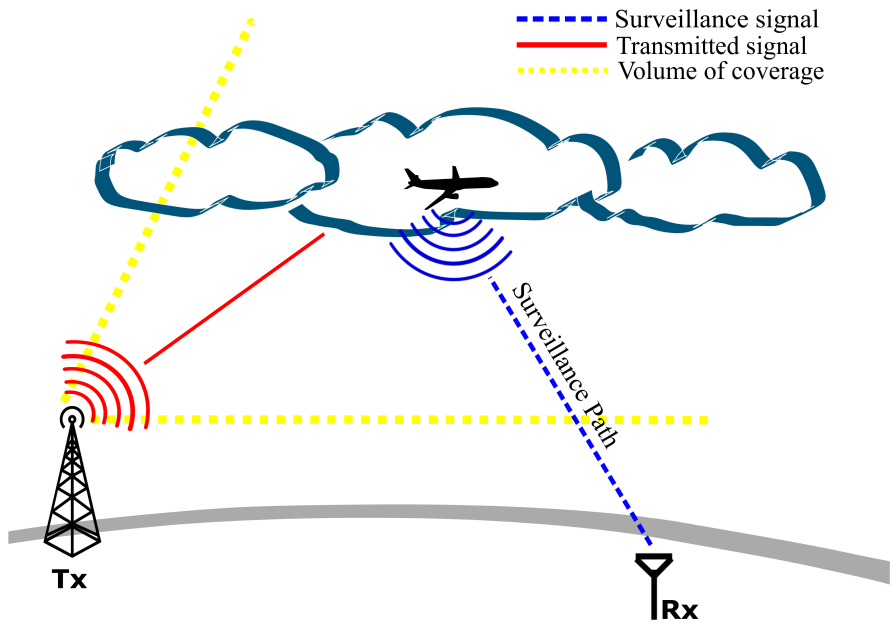

Figure 2: In weather surveillance radar, due to the high elevation angle and corresponding volume coverage pattern (VCP), minimal direct-path signal is observed by the receiver located on the ground in the reference channel.

Signal Model: Electromagnetic Vector Sensors

- Let (θ, ϕ) denote the azimuth and elevation angle, respectively, of a hypothesized target located at $\boldsymbol{p} = [p_{\mathrm{x}}, p_{\mathrm{y}}, p_{\mathrm{z}}]^T \in \mathbb{R}^3$ and traveling with a velocity $\dot{\boldsymbol{p}} = [\dot{p}_{\mathrm{x}}, \dot{p}_{\mathrm{y}}, \dot{p}_{\mathrm{z}}]^T \in \mathbb{R}^3$, as seen by the receiver. The steering matrix of an EMVS denoted as $\boldsymbol{D}_{\theta,\phi} \in \mathbb{R}^{6\times 2}$ can be parameterized[1] as

$$\boldsymbol{D}_{\theta,\phi} = \begin{bmatrix} -\sin\theta & -\cos\theta\sin\phi \\ \cos\theta & -\sin\theta\sin\phi \\ 0 & \cos\phi \\ -\cos\theta\sin\phi & \sin\phi \\ -\sin\theta\sin\phi & -\cos\phi \\ \cos\phi & 0 \end{bmatrix}. \tag{2}$$

The inner product of the steering matrix $\boldsymbol{D}_{\theta,\phi}^H \boldsymbol{D}_{\theta,\phi} = k\boldsymbol{I}_6$, where $k = 2$ for EMVS[2].

[1] A. Nehorai, E. Paldi, "Vector-sensor array processing for electromagnetic source localization", *IEEE Transactions on Signal Processing*, vol. 42, pp. 376–398, Feb. 1994.

[2] For a tripole antenna and a classical polarization radar using vertical and horizontal linear polarization, $k = 1$.

Signal Model: Scattering Matrix and Polarization

- Let $\boldsymbol{S}_{\mathrm{p}} \in \mathbb{C}^{2\times 2}$ and $\boldsymbol{S}_{\mathrm{c}} \in \mathbb{C}^{2\times 2}$ denote the hypothesized target and clutter scattering matrix coefficients, respectively, as seen by the receiver located at coordinates $\boldsymbol{r} = [r_{\mathrm{x}}, r_{\mathrm{y}}, r_{\mathrm{z}}]^T \in \mathbb{R}^3$, where $\boldsymbol{S}_{\mathrm{p}}$ and $\boldsymbol{S}_{\mathrm{c}}$ are parameterized as

$$\boldsymbol{S}_{\mathrm{p}} = \begin{bmatrix} \sigma_{\mathrm{p}}^{\mathrm{hh}} & \sigma_{\mathrm{p}}^{\mathrm{hv}} \\ \sigma_{\mathrm{p}}^{\mathrm{vh}} & \sigma_{\mathrm{p}}^{\mathrm{vv}} \end{bmatrix} \quad \text{and} \quad \boldsymbol{S}_{\mathrm{c}} = \begin{bmatrix} \sigma_{\mathrm{c}}^{\mathrm{hh}} & \sigma_{\mathrm{c}}^{\mathrm{hv}} \\ \sigma_{\mathrm{c}}^{\mathrm{vh}} & \sigma_{\mathrm{c}}^{\mathrm{vv}} \end{bmatrix}. \tag{3}$$

- The polarimetric representation of the transmitted complex bandpass signal is given by $\boldsymbol{Q}_{\alpha}\boldsymbol{w}_{\beta}\, s(t) e^{j\Omega_{\mathrm{C}} t}$ where

$$\boldsymbol{Q}_{\alpha} = \begin{bmatrix} \cos\alpha & \sin\alpha \\ -\sin\alpha & \cos\alpha \end{bmatrix}, \quad \boldsymbol{w}_{\beta} = \begin{bmatrix} \cos\beta \\ j\sin\beta \end{bmatrix}, \tag{4}$$

  and α and β represent the orientation and ellipticity of the transmitted signal, respectively, and Ω_{C} is the carrier frequency.

Signal Model: EMVS Receiver

- The signal $s(t)$ is the complex baseband signal, $t \in [0, T]$, where $T/2$ is the pulse repetition interval (PRI) of a dual-polarized transmitter, which sends sequentially two pulses of orthogonal polarization.
- The complex envelope signal at the output of the quadrature receiver can be expressed as

$$\begin{aligned} \boldsymbol{y}(t) = & \underbrace{\boldsymbol{D}_{\theta,\phi}\boldsymbol{S}_{\mathrm{p}}\boldsymbol{Q}_{\alpha}\boldsymbol{w}_{\beta}\, s(t-\tau_{\mathrm{p}})e^{j\Omega_{\mathrm{D}}t}e^{-j\Omega_{\mathrm{C}}\tau_{\mathrm{p}}}}_{\text{target signal}} \\ & + \underbrace{\boldsymbol{D}_{\theta,\phi}\boldsymbol{S}_{\mathrm{c}}\boldsymbol{Q}_{\alpha}\boldsymbol{w}_{\beta}\, s(t-\tau_{\mathrm{c}})e^{-j\Omega_{\mathrm{C}}\tau_{\mathrm{c}}}}_{\text{clutter signal}} + \underbrace{\boldsymbol{e}(t)}_{\text{noise}}, \end{aligned} \tag{5}$$

where

$$\Omega_{\mathrm{D}} = \frac{\Omega_{\mathrm{C}}}{c}\left[\frac{(\boldsymbol{r}-\boldsymbol{p})^T\dot{\boldsymbol{p}}}{\|\boldsymbol{r}-\boldsymbol{p}\|} + \frac{(\boldsymbol{p}-\boldsymbol{t})^T\dot{\boldsymbol{p}}}{\|\boldsymbol{p}-\boldsymbol{t}\|}\right], \quad \text{and} \quad \tau_{\mathrm{p}} = \frac{\|\boldsymbol{r}-\boldsymbol{p}\| + \|\boldsymbol{p}-\boldsymbol{t}\|}{c}. \tag{6}$$

- Here, τ_{p} and τ_{c} represents target and the clutter delay, respectively, Ω_{D} represents the Doppler shift in the signal, c is the speed of the propagation of the electromagnetic wave.

Signal Model: EMVS Receiver (Cont.)

- We assume that τ_{c} is known and is approximately equal to the time it takes for the echo signal to travel from the center of the range cell to the receiver.

- It is reasonable to assume that the receiver has a good prior knowledge of the Doppler frequency shift produced by clutter through Level II and Level III weather radar data products, which are available for commercial applications and updated regularly.

- Based on this assumptions, $\tau_{\mathrm{p}} = \tau_{\mathrm{c}} + \Delta\tau_{\mathrm{p}}$, where $\Delta\tau_{\mathrm{p}}$ accounts for the shift in the target's position from the center of the range cell. Compensating for the absolute phase term $e^{-j\Omega_{\mathrm{C}}\tau_{\mathrm{c}}}$, the received signal in (5) can be written as

$$\begin{aligned}\boldsymbol{y}(t) = &\underbrace{\boldsymbol{D}_{\theta,\phi}\boldsymbol{S}_{\mathrm{p}}\boldsymbol{Q}_{\alpha}\boldsymbol{w}_{\beta}\, s(t-\tau_{\mathrm{p}})e^{j\Omega_{\mathrm{D}}t}e^{-j\Omega_{\mathrm{C}}\Delta\tau_{\mathrm{p}}}}_{\text{target signal}} \\ &+ \underbrace{\boldsymbol{D}_{\theta,\phi}\boldsymbol{S}_{\mathrm{c}}\boldsymbol{Q}_{\alpha}\boldsymbol{w}_{\beta}\, s(t-\tau_{\mathrm{c}})}_{\text{clutter signal}} + \underbrace{\boldsymbol{e}(t)}_{\text{noise}}\,.\end{aligned} \tag{7}$$

Signal Model: EMVS Receiver (Cont.)

- We introduce the vectorized scattering matrix coefficients, $\boldsymbol{x}_{\mathrm{p}} = e^{-j\Omega_{\mathrm{C}}\Delta\tau_{\mathrm{p}}}[\sigma_{\mathrm{p}}^{hh}, \sigma_{\mathrm{p}}^{vv}, \sigma_{\mathrm{p}}^{hv}, \sigma_{\mathrm{p}}^{vh}]^T$ and $\boldsymbol{x}_{\mathrm{c}} = [\sigma_{\mathrm{c}}^{hh}, \sigma_{\mathrm{c}}^{vv}, \sigma_{\mathrm{c}}^{hv}, \sigma_{\mathrm{c}}^{vh}]^T$, that denote the target and clutter reflectivity coefficients, respectively.

- Let $\boldsymbol{\epsilon}_{\alpha,\beta} \triangleq [\epsilon_1, \epsilon_2]^T = \boldsymbol{Q}_{\alpha}\boldsymbol{w}_{\beta}$ denote the polarization vector. We define polarization matrix[3] as

$$\bar{\boldsymbol{\epsilon}}_{\alpha,\beta} = \begin{bmatrix} \epsilon_1 & 0 & \epsilon_2 & 0 \\ 0 & \epsilon_2 & 0 & \epsilon_1 \end{bmatrix}, \tag{8}$$

  where $\mathrm{rank}(\bar{\boldsymbol{\epsilon}}_{\alpha,\beta}) = 2$. Then, the received signal in (7) can be rewritten as

$$\boldsymbol{y}(t) = \boldsymbol{D}_{\theta,\phi}\bar{\boldsymbol{\epsilon}}_{\alpha,\beta}\boldsymbol{x}_{\mathrm{p}}s(t-\tau_{\mathrm{p}})e^{j\Omega_{\mathrm{D}}t} + \boldsymbol{D}_{\theta,\phi}\bar{\boldsymbol{\epsilon}}_{\alpha,\beta}\boldsymbol{x}_{\mathrm{c}}s(t-\tau_{\mathrm{c}}) + \boldsymbol{e}(t). \tag{9}$$

- Discretization: The received signal is sampled at a fast-time sampling interval Δt seconds.

$$\boldsymbol{y}[n] = \boldsymbol{D}_{\theta,\phi}\bar{\boldsymbol{\epsilon}}_{\alpha,\beta}\boldsymbol{x}_{\mathrm{p}}s[n-n_{\mathrm{p}}]e^{j\omega_{\mathrm{D}}n} + \boldsymbol{D}_{\theta,\phi}\bar{\boldsymbol{\epsilon}}_{\alpha,\beta}\boldsymbol{x}_{\mathrm{c}}s[n-n_{\mathrm{c}}] + \boldsymbol{e}[n]. \tag{10}$$

  where $n_{\mathrm{p}} = \tau_{\mathrm{p}}/\Delta t$, $n_{\mathrm{c}} = \tau_{\mathrm{c}}/\Delta t$, and $\omega_{\mathrm{D}} = \Omega_{\mathrm{D}}\Delta t$.

[3] M. Hurtado and A. Nehorai, "Polarimetric detection of targets in heavy inhomogeneous clutter", *IEEE Transactions on Signal Processing*, vol. 56, pp. 1349–1361, Apr. 2008.

Signal Model: EMVS Receiver (Cont.)

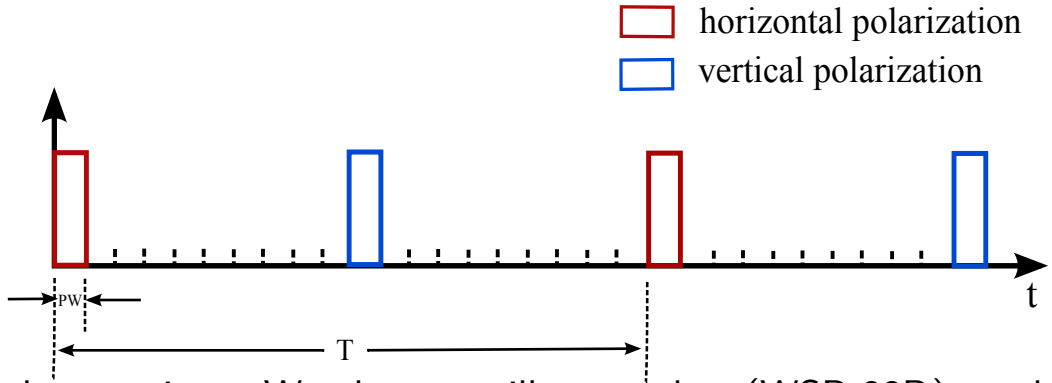

Figure 3: Dual-polarized transmitter. Weather surveillance radars (WSR-88D) employ alternating transmission of horizontal and vertical polarized waveforms.

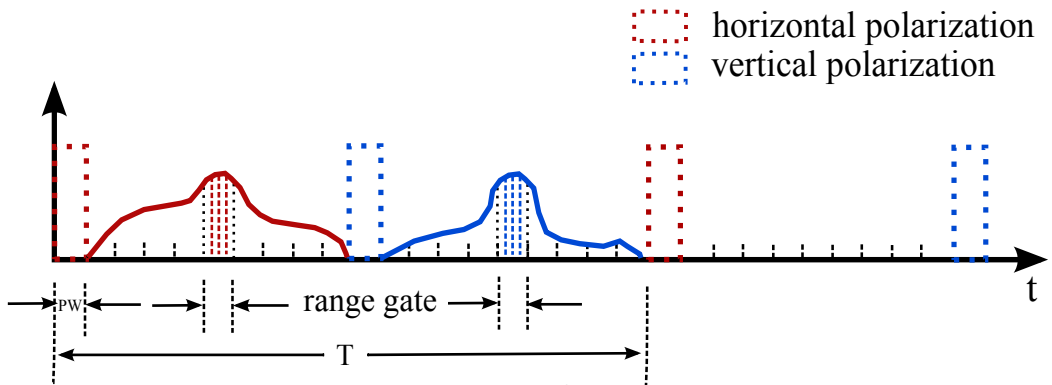

Figure 4: An illustration of the sampling scheme.

Signal Model: EMVS Receiver (Cont.)

- The received signal[4] in (10) can be represented as

$$\boldsymbol{y} = \underbrace{(\mathcal{D}_{n_\mathrm{p},\omega_\mathrm{D}} \otimes \boldsymbol{D}_{\theta,\phi})(\boldsymbol{s} \otimes \bar{\boldsymbol{\epsilon}}_{\alpha,\beta})\boldsymbol{x}_\mathrm{p}}_{\text{target signal}} + \underbrace{(\mathcal{D}_{n_\mathrm{c},0} \otimes \boldsymbol{D}_{\theta,\phi})(\boldsymbol{s} \otimes \bar{\boldsymbol{\epsilon}}_{\alpha,\beta})\boldsymbol{x}_\mathrm{c}}_{\text{clutter signal}} + \underbrace{\boldsymbol{e}}_{\text{noise}}$$

$$= \boldsymbol{B}\boldsymbol{S}\boldsymbol{x}_\mathrm{p} + \boldsymbol{A}\boldsymbol{S}\boldsymbol{x}_\mathrm{c} + \boldsymbol{e}. \tag{11}$$

where

- $\boldsymbol{s} = [s(0), \ldots, s(N-1)]^T$ is the transmitted signal vector,
- $\boldsymbol{S} = \boldsymbol{s} \otimes \bar{\boldsymbol{\epsilon}}_{\alpha,\beta} \in \mathbb{C}^{M \times P}$ is the signal information matrix,
- $\mathcal{D}_{n,\omega} = \boldsymbol{L}_N(\omega)\boldsymbol{F}_N^H \boldsymbol{L}_N(-2\pi n/N)\boldsymbol{F}_N$ is the delay-Doppler matrix[5],
- $\boldsymbol{F}_N \in \mathbb{C}^{N \times N}$ denote the unitary discrete Fourier transform (DFT) matrix,
- $\boldsymbol{L}_N(x) = \mathrm{diag}\{e^{j(0)x}, e^{j(1)x}, \ldots, e^{j(N-1)x}\}$ is a diagonal matrix,
- $\boldsymbol{A} = \mathcal{D}_{n_\mathrm{c},0} \otimes \boldsymbol{D}_{\theta,\phi} \in \mathbb{C}^{L \times M}$ and $\boldsymbol{A}^H\boldsymbol{A} = k\boldsymbol{I}_M$, and
- $\boldsymbol{B} = \mathcal{D}_{n_\mathrm{p},\omega_\mathrm{D}} \otimes \boldsymbol{D}_{\theta,\phi} \in \mathbb{C}^{L \times M}$ and $\boldsymbol{B}^H\boldsymbol{B} = k\boldsymbol{I}_M$.

[4] For an EMVS receiver, $L = 6N$, $M = 2N$, $P = 4$, and $k = 2$. For a tripole antenna $L = 3N$, $M = 2N$, $P = 4$, and $k = 1$. For a classical polarization radar using vertical and horizontal linear polarization $L = 2N$, $M = 2N$, $P = 4$, and $k = 1$.

[5] D. E. Hack, L. K. Patton, B. Himed and M. A. Saville, "Centralized passive MIMO radar detection without direct-path reference signals," in *IEEE Transactions on Signal Processing*, vol. 62, pp. 3013-3023, June 2014.

Signal Model and Statistics

- Based on the statistics of the target, clutter, and noise as mentioned above, the received signal vector at the receiver for a moving target, denoted as $\boldsymbol{y}_d \in \mathbb{C}^{L\times 1}$ is a complex Gaussian distributed as

$$\begin{aligned}\mathcal{H}_0 &: \boldsymbol{y}_d \sim \mathcal{CN}\left(\boldsymbol{0}, \boldsymbol{A}\boldsymbol{S}\boldsymbol{\Sigma}\boldsymbol{S}^H\boldsymbol{A}^H + \sigma\boldsymbol{I}_L\right)\\ \mathcal{H}_1 &: \boldsymbol{y}_d \sim \mathcal{CN}\left(\boldsymbol{B}\boldsymbol{S}\boldsymbol{\mu}, \boldsymbol{A}\boldsymbol{S}\boldsymbol{\Sigma}\boldsymbol{S}^H\boldsymbol{A}^H + \sigma\boldsymbol{I}_L\right),\end{aligned} \tag{12}$$

  where
  - d represents the snapshot index,
  - $\boldsymbol{S}$ is the signal information matrix is *deterministic* and *unknown*,
  - scattering coefficients of the clutter, $\boldsymbol{x}_c$, are assumed to be distributed as zero mean complex Gaussian random vectors with *unknown* covariance matrices denoted as $\boldsymbol{\Sigma}$,
  - polarimetric scattering matrix of the target is rearranged in a coefficient vector, which is assumed deterministic and *unknown*, i.e., $\mathbb{E}[\boldsymbol{x}_{\mathrm{p}}] = \boldsymbol{\mu}$ is unknown, and
  - receiver noise vector, $\boldsymbol{e}$, is a zero mean complex Gaussian random vector with covariance $\sigma\boldsymbol{I}_L$, where we assume σ is *known*.

Outline

- Passive radar
- Signal model and statistics
- Generalized likelihood ratio test detector
- Numerical results
- Future work

Generalized Likelihood Ratio Test

- In GLRT, the parameters which are assumed to be deterministic and unknown, are replaced with their maximum likelihood estimate (MLE). This method may not always be optimal, but it works well in practice. The GLRT detector is written as

$$\begin{aligned} \max_{\{\boldsymbol{\Sigma},\boldsymbol{\mu},\boldsymbol{S}\}} \ln f_1(\boldsymbol{\Sigma},\boldsymbol{\mu},\boldsymbol{S}) - \max_{\{\boldsymbol{\Sigma},\boldsymbol{S}\}} \ln f_0(\boldsymbol{\Sigma},\boldsymbol{S}) \\ = \ln f_1(\hat{\boldsymbol{\Sigma}}_1,\hat{\boldsymbol{\mu}},\hat{\boldsymbol{S}}) - \ln f_0(\hat{\boldsymbol{\Sigma}}_0,\hat{\boldsymbol{S}}) \gtrless \ln \kappa, \end{aligned} \tag{13}$$

  where $\ln f_0(\boldsymbol{\Sigma},\boldsymbol{S})$ and $\ln f_1(\boldsymbol{\Sigma},\boldsymbol{\mu},\boldsymbol{S})$ are the log-likelihood ratio of the probability density functions under each hypothesis in (12), and κ is the detection threshold.

Lemma: MLE of the Clutter Covariance Matrix

Lemma 1. *The Hermitian matrix $\boldsymbol{\Sigma}$ that maximizes*

$$-D\left[L\ln\pi+\ln|\boldsymbol{\Gamma}|+\mathrm{Tr}\{\boldsymbol{\Gamma}^{-1}\boldsymbol{R}\}\right]$$

where $\boldsymbol{\Gamma}=\boldsymbol{A}\boldsymbol{S}\boldsymbol{\Sigma}\boldsymbol{S}^{H}\boldsymbol{A}^{H}+\sigma\boldsymbol{I}_{L}$ is the true covariance matrix, $\boldsymbol{R}$ is the sample covariance matrix, L is the number of samples, and D is the number of snapshots, is given as

$$\hat{\boldsymbol{\Sigma}}=(\boldsymbol{A}\boldsymbol{S})^{\dagger}\boldsymbol{R}(\boldsymbol{A}\boldsymbol{S})^{\dagger\,H}-\sigma(\boldsymbol{S}^{H}\boldsymbol{A}^{H}\boldsymbol{A}\boldsymbol{S}). \tag{14}$$

Proof. *See Theorem*[6] *1.1 (or) Appendix*[7] *A.* □

[6] P. Stoica and A. Nehorai, "On the concentrated stochastic likelihood function in array signal processing", *Circ. Sys. Signal Processing*, Vol. 14, No. 5, pp. 669-674, 1995.

[7] G.V. Prateek, M. Hurtado and A. Nehorai, "Target detection using weather radars and electromagnetic vector sensors," *Signal Processing*, Vol. 137, pp. 387-397, Aug. 2017.

Lemma: Trace Approximation

Lemma 2. *For sufficiently large number of snapshots D,*

$$\sigma^{-1}\,\mathrm{Tr}\{\boldsymbol{P}_{\mathrm{AS}}^{\perp}\boldsymbol{R}\} \approx L - P$$

where $\boldsymbol{P}_{\mathrm{AS}}^{\perp}$ is the orthogonal projection matrix and is given as

$$\boldsymbol{P}_{\mathrm{AS}}^{\perp} = \boldsymbol{I}_L - \boldsymbol{P}_{\mathrm{AS}} = \boldsymbol{I}_L - \boldsymbol{A}\boldsymbol{S}(\boldsymbol{S}^H\boldsymbol{A}^H\boldsymbol{A}\boldsymbol{S})^{-1}\boldsymbol{S}^H\boldsymbol{A}^H.$$

and $\mathrm{rank}(\boldsymbol{S}) = \mathrm{rank}(\boldsymbol{P}_{\mathrm{AS}}) = P$.

Proof. *The sample covariance matrix converges to the true covariance matrix in an asymptotic sense, as the number of snapshots increases. We replace the sample covariance matrix $\boldsymbol{R}$ in $\sigma^{-1}\,\mathrm{Tr}\{\boldsymbol{P}_{\mathrm{AS}}^{\perp}\boldsymbol{R}\}$ with $\boldsymbol{\Gamma}$, and then expand as follows*[8]*:*

$$\begin{aligned}
\sigma^{-1}\,\mathrm{Tr}\{\boldsymbol{P}_{\mathrm{AS}}^{\perp}\boldsymbol{R}\} &\approx \sigma^{-1}\,\mathrm{Tr}\{\boldsymbol{P}_{\mathrm{AS}}^{\perp}\boldsymbol{\Gamma}\}, \quad \textit{for } D \gg L \\
&= \sigma^{-1}\,\mathrm{Tr}\{(\boldsymbol{I}_L - \boldsymbol{P}_{\mathrm{AS}})\boldsymbol{\Gamma}\} \\
&= \sigma^{-1}\,\mathrm{Tr}\{\boldsymbol{\Gamma} - \boldsymbol{P}_{\mathrm{AS}}\boldsymbol{\Gamma}\} \\
&= L - P.
\end{aligned}$$

□

[8] G.V. Prateek, M. Hurtado and A. Nehorai, "Target detection using weather radars and electromagnetic vector sensors," *Signal Processing*, Vol. 137, pp. 387-397, Aug. 2017.

Null Hypothesis

- Based on (12), the loglikelihood function with respect to the unknown parameters $\boldsymbol{S}$ and $\boldsymbol{\Sigma}$ under the hypothesis $\mathcal{H}_0$ is expressed as

$$\ln f_0(\boldsymbol{\Sigma}, \boldsymbol{S}) = -D\left[L \ln \pi + \ln |\boldsymbol{\Gamma}| + \mathrm{Tr}\{\boldsymbol{\Gamma}^{-1}\boldsymbol{R}_0\}\right], \tag{15}$$

  where D is the number of snapshots, and $\boldsymbol{R}_0$ is the sample covariance matrix under hypothesis $\mathcal{H}_0$ given as

$$\boldsymbol{R}_0 = \frac{1}{D}\sum_{d=1}^{D} \boldsymbol{y}_d \boldsymbol{y}_d^H, \quad D \gg L. \tag{16}$$

- Applying Lemma 1 and Lemma 2, the loglikelihood function can be further simplified as

$$\begin{aligned}\ln f_0(\hat{\boldsymbol{\Sigma}}_0, \boldsymbol{S}) \approx -D\Big[&L + L\ln\pi + (L-P)\ln\sigma + \ln\left|\boldsymbol{S}^H\boldsymbol{A}^H\boldsymbol{R}_0\boldsymbol{A}\boldsymbol{S}\right| \\ &- \ln|\boldsymbol{S}^H\boldsymbol{A}^H\boldsymbol{A}\boldsymbol{S}|\Big].\end{aligned} \tag{17}$$

Lemma: MLE of the Signal Information Matrix

Lemma 3. *The Unitary matrix $\boldsymbol{S}$ that maximizes*

$$-D\left[L + L\ln\pi + (L-P)\ln\sigma + \ln\left|\boldsymbol{S}^H\boldsymbol{A}^H\boldsymbol{R}\boldsymbol{A}\boldsymbol{S}\right| - \ln\left|\boldsymbol{S}^H\boldsymbol{A}^H\boldsymbol{A}\boldsymbol{S}\right|\right],$$

is given by $\boldsymbol{W}_1$, where $\boldsymbol{W}\boldsymbol{\Xi}\boldsymbol{W}^H$ is the orthogonal factorization of $\boldsymbol{A}^H\boldsymbol{R}\boldsymbol{A}$, $\boldsymbol{W}$ is an orthogonal matrix partitioned as $[\boldsymbol{W}_1, \boldsymbol{W}_2]$, such that $\boldsymbol{W}_1 \in \mathbb{C}^{M\times P}$ and $\boldsymbol{W}_2 \in \mathbb{C}^{M\times(L-P)}$, and $\boldsymbol{W}_1$ represents the eigenvectors corresponding to P largest eigenvalues of $\boldsymbol{A}^H\boldsymbol{R}\boldsymbol{A}$.

Proof. *See Appendix*[9] *C.* □

[9] G.V. Prateek, M. Hurtado and A. Nehorai, "Target detection using weather radars and electromagnetic vector sensors," *Signal Processing*, Vol. 137, pp. 387-397, Aug. 2017.

Null Hypothesis (Cont.)

- Let $\boldsymbol{U}\boldsymbol{\Omega}\boldsymbol{U}^H$ be the orthogonal factorization of $\boldsymbol{A}^H\boldsymbol{R}_0\boldsymbol{A}$, where $\boldsymbol{U}$ contains orthogonal column vectors such that $\boldsymbol{U}\boldsymbol{U}^H = \boldsymbol{I}_M$, and $\boldsymbol{\Omega}$ is a diagonal matrix with eigenvalues of $\boldsymbol{A}^H\boldsymbol{R}_0\boldsymbol{A}$ as its diagonal entries, arranged in decreasing order.

- We partition the orthogonal column vectors of $\boldsymbol{U}$ as $\begin{bmatrix}\boldsymbol{U}_1 & \boldsymbol{U}_2\end{bmatrix}$, such that $\boldsymbol{U}_1 \in \mathbb{C}^{M\times P}$, $\boldsymbol{U}_2 \in \mathbb{C}^{M\times(L-P)}$.

- Applying Lemma 3, we get

$$\begin{aligned}\ln f_0(\hat{\boldsymbol{\Sigma}}_0, \hat{\boldsymbol{S}}) = -D\,[&L + L\ln\pi + (L-P)\ln\sigma - \ln|k\boldsymbol{I}_P| \\ &+ \ln\left|\boldsymbol{U}_1^H\boldsymbol{A}^H\boldsymbol{R}_0\boldsymbol{A}\boldsymbol{U}_1\right|\Big]\,.\end{aligned} \tag{18}$$

Alternative Hypothesis

- Following a similar approach, the loglikelihood function with respect to the unknown parameters $\boldsymbol{\Sigma}$, $\boldsymbol{\mu}$, and $\boldsymbol{S}$ under hypothesis $\mathcal{H}_1$ in (12), is expressed as

$$\ln f_1(\boldsymbol{\Sigma}, \boldsymbol{\mu}, \boldsymbol{S}) = -D \left[L \ln \pi + \ln |\boldsymbol{\Gamma}| + \mathrm{Tr}\{\boldsymbol{\Gamma}^{-1} \boldsymbol{R}_1\} \right], \tag{19}$$

  where $\boldsymbol{R}_1$ is the sample covariance matrix under $\mathcal{H}_1$, given as

$$\boldsymbol{R}_1 = \frac{1}{D} \sum_{d=1}^{D} (\boldsymbol{y}_d - \boldsymbol{B}\boldsymbol{S}\boldsymbol{\mu})(\boldsymbol{y}_d - \boldsymbol{B}\boldsymbol{S}\boldsymbol{\mu})^H \quad D \gg L. \tag{20}$$

- Applying Lemma 1 and Lemma 2, and further simplifying, we get

$$\begin{aligned} \ln f_1(\hat{\boldsymbol{\Sigma}}_1, \boldsymbol{\mu}, \boldsymbol{S}) \approx -D \Big[& L + L \ln \pi + (L - P) \ln \sigma - \ln \left| \boldsymbol{S}^H \boldsymbol{A}^H \boldsymbol{A} \boldsymbol{S} \right| \\ & + \ln \left| \boldsymbol{S}^H \boldsymbol{A}^H \boldsymbol{R}_1 \boldsymbol{A} \boldsymbol{S} \right| \Big]. \end{aligned} \tag{21}$$

Lemma: MLE of the Target Scattering Matrix Coefficient

Lemma 4. *The maximum likelihood estimate of* $\ln \left| \boldsymbol{S}^H \boldsymbol{A}^H \boldsymbol{R}_1 \boldsymbol{A} \boldsymbol{S} \right|$, *where*

$$\boldsymbol{R}_1 = \frac{1}{D} \sum_{d=1}^{D} (\boldsymbol{y}_d - \boldsymbol{B}\boldsymbol{S}\boldsymbol{\mu})(\boldsymbol{y}_d - \boldsymbol{B}\boldsymbol{S}\boldsymbol{\mu})^H$$

is given as $\hat{\boldsymbol{\mu}} = (\boldsymbol{B}\boldsymbol{S})^{\dagger} \bar{\boldsymbol{y}}$, *where* $\bar{\boldsymbol{y}} = \frac{1}{D} \sum_{d=1}^{D} \boldsymbol{y}_d$.

Proof. *See Appendix*[10] *D.* □

Using Lemma 4, we get the following approximation

$$\ln \left| \boldsymbol{S}^H \boldsymbol{A}^H \boldsymbol{R}_1 \boldsymbol{A} \boldsymbol{S} \right| \approx \ln \left| \boldsymbol{S}^H \boldsymbol{A}^H \boldsymbol{R}_2 \boldsymbol{A} \boldsymbol{S} \right| \quad \text{(because } \bar{\boldsymbol{y}} \to \boldsymbol{B}\boldsymbol{S}\boldsymbol{\mu} \text{ and } \boldsymbol{P}_{\mathrm{BS}}^{\perp} \bar{\boldsymbol{y}} \approx \boldsymbol{0}\text{)} \quad (22)$$

where $\boldsymbol{R}_2 \triangleq (\boldsymbol{R}_0 - \bar{\boldsymbol{y}}\bar{\boldsymbol{y}}^H) = \frac{1}{D} \sum_{d=1}^{D} (\boldsymbol{y}_d - \bar{\boldsymbol{y}})(\boldsymbol{y}_d - \bar{\boldsymbol{y}})^H$.

[10] G.V. Prateek, M. Hurtado and A. Nehorai, "Target detection using weather radars and electromagnetic vector sensors," *Signal Processing*, Vol. 137, pp. 387-397, Aug. 2017.

Alternative Hypothesis (Cont.)

- Let $\boldsymbol{V}\boldsymbol{\Upsilon}\boldsymbol{V}^H$ be the orthogonal factorization of $\boldsymbol{A}^H\boldsymbol{R}_2\boldsymbol{A}$, where $\boldsymbol{V}$ represents the orthogonal column vectors such that $\boldsymbol{V}\boldsymbol{V}^H = \boldsymbol{I}_M$, and $\boldsymbol{\Upsilon}$ is a diagonal matrix with eigenvalues of $\boldsymbol{A}^H\boldsymbol{R}_2\boldsymbol{A}$ as its diagonal entries, arranged in descending order.

- We partition the orthogonal column vectors of $\boldsymbol{V}$ as $\begin{bmatrix}\boldsymbol{V}_1 & \boldsymbol{V}_2\end{bmatrix}$, such that $\boldsymbol{V}_1 \in \mathbb{C}^{M\times P}$, $\boldsymbol{V}_2 \in \mathbb{C}^{M\times(L-P)}$.

- Applying Lemma 3, we get

$$\begin{aligned}\ln f_1(\hat{\boldsymbol{\Sigma}}_1, \hat{\boldsymbol{\mu}}, \hat{\boldsymbol{S}}) = -D\,[&L + L\ln\pi + (L-P)\ln\sigma - \ln|k\boldsymbol{I}_P| \\ &+ \ln\left|\boldsymbol{V}_1^H\boldsymbol{A}^H\boldsymbol{R}_2\boldsymbol{A}\boldsymbol{V}_1\right|\Big].\end{aligned} \tag{23}$$

GLRT Detector

- Substituting (18) and (23) into (13), the GLRT is given as

$$D\left[\ln\left|\boldsymbol{U}_1^H\boldsymbol{A}^H\boldsymbol{R}_0\boldsymbol{A}\boldsymbol{U}_1\right| - \ln\left|\boldsymbol{V}_1^H\boldsymbol{A}^H\boldsymbol{R}_2\boldsymbol{A}\boldsymbol{V}_1\right|\right] \gtrless \ln\kappa. \tag{24}$$

- The GLRT in (24) can be rewritten as

$$\begin{aligned} D\Big[&\ln(1+\bar{\boldsymbol{y}}^H\boldsymbol{A}\boldsymbol{U}_1(\boldsymbol{U}_1^H\boldsymbol{A}^H\boldsymbol{R}_2\boldsymbol{A}\boldsymbol{U}_1)^{-1}\boldsymbol{U}_1^H\boldsymbol{A}^H\bar{\boldsymbol{y}})+ \\ &\ln\left|\boldsymbol{U}_1^H\boldsymbol{A}^H\boldsymbol{R}_2\boldsymbol{A}\boldsymbol{U}_1\right| - \ln\left|\boldsymbol{V}_1^H\boldsymbol{A}^H\boldsymbol{R}_2\boldsymbol{A}\boldsymbol{V}_1\right|\Big] \gtrless \ln\kappa. \end{aligned} \tag{25}$$

- The matrices $\boldsymbol{U}_1$ and $\boldsymbol{V}_1$ represent the eigenvectors corresponding to the P largest eigenvalues of $\boldsymbol{A}^H\boldsymbol{R}_0\boldsymbol{A}$ and $\boldsymbol{A}^H\boldsymbol{R}_2\boldsymbol{A}$, respectively. When we have a large number of snapshots, both $\boldsymbol{R}_0$ and $\boldsymbol{R}_2$ converge to the true covariance matrix, $\boldsymbol{\Gamma}$. Hence, the eigenvectors corresponding to P largest eigenvalues of $\boldsymbol{A}^H\boldsymbol{R}_0\boldsymbol{A}$ and $\boldsymbol{A}^H\boldsymbol{R}_2\boldsymbol{A}$ also converge.

GLRT Detector (Cont.)

- Based on this asymptotic property of sample covariance matrix we replace $\boldsymbol{V}_1$ with $\boldsymbol{U}_1$ in (25). Then, the GLRT statistic can be written as

$$D[\ln(1+\bar{\boldsymbol{y}}^H \boldsymbol{A}\boldsymbol{U}_1(\boldsymbol{U}_1^H \boldsymbol{A}^H \boldsymbol{R}_2 \boldsymbol{A}\boldsymbol{U}_1)^{-1}\boldsymbol{U}_1^H \boldsymbol{A}^H \bar{\boldsymbol{y}})] \gtrless \ln \kappa. \tag{26}$$

- Let $\boldsymbol{z}_d = \boldsymbol{U}_1^H \boldsymbol{A}^H \boldsymbol{y}_d$. The new sample mean and sample covariance are $\bar{\boldsymbol{z}} = \frac{1}{D}\sum_{d=1}^{D} \boldsymbol{z}_d$ and $\boldsymbol{R}_{\boldsymbol{z}} = \frac{1}{D}\sum_{d=1}^{D}(\boldsymbol{z}_d - \bar{\boldsymbol{z}})(\boldsymbol{z}_d - \bar{\boldsymbol{z}})^H$, respectively. Hence, the decision test statistic in (26) is given as

$$D \ln(1+\bar{\boldsymbol{z}}^H \boldsymbol{R}_{\boldsymbol{z}}^{-1}\bar{\boldsymbol{z}}) \gtrless \ln \kappa. \tag{27}$$

- Removing the logarithm and ignoring the constant term, the equivalent test statistic is

$$\xi = \bar{\boldsymbol{z}}^H \boldsymbol{R}_{\boldsymbol{z}}^{-1}\bar{\boldsymbol{z}}. \tag{28}$$

Distribution of Test Statistic

- The test statistic in (28) is distributed as follows:

$$\frac{2(D-P)}{2P}\xi \sim \begin{cases} \mathcal{F}_{2P,2(D-P)}, & \text{under } \mathcal{H}_0 \\ \mathcal{F}_{2P,2(D-P)}(\lambda), & \text{under } \mathcal{H}_1 \end{cases}. \tag{29}$$

- As D increases, the degrees of freedom ν_2 also increases, and the F-distribution $\mathcal{F}_{\nu_1,\nu_2}$ can be approximated as a chi-square distribution denoted by $\chi^2_{\nu_1}$.

$$2(D-P)\xi \sim \begin{cases} \chi^2_{2P}, & \text{under } \mathcal{H}_0 \\ \chi^2_{2P}(\lambda), & \text{under } \mathcal{H}_1 \end{cases}, \tag{30}$$

- The non-centrality parameter is given as

$$\lambda = 2D\boldsymbol{\mu}^H \boldsymbol{S}^H \boldsymbol{B}^H \boldsymbol{A}\boldsymbol{U}_1[\boldsymbol{U}_1^H \boldsymbol{A}^H \boldsymbol{\Gamma} \boldsymbol{A}\boldsymbol{U}_1]^{-1}\boldsymbol{U}_1^H \boldsymbol{A}^H \boldsymbol{B}\boldsymbol{S}\boldsymbol{\mu} \tag{31}$$

- The probability of false alarm does not depend on the transmitted signal, clutter, and noise, indicating the constant false alarm rate (CFAR) of the detector.

Outline

- Passive radar
- Signal model and statistics
- Generalized likelihood ratio test detector
- Numerical results
- Future work

Numerical Results: Simulation Settings

Problem:
Detect a moving target in the presence of signal-dependent clutter.

Transmitter specifications:

Table 1: Dual-polarized transmitter specifications with velocity as the characteristic of interest.

Parameter	Value
Carrier frequency	$2.7\,\mathrm{GHz}$
Bandwidth	$0.63\,\mathrm{MHz}$
Beam width	0.96°
Pulse width	$1.5\mu\,\mathrm{s}$ (short pulse)
Pulse repetition frequency	$322 - 1282\,\mathrm{Hz}$
Range of Observation	$230\,\mathrm{km}$ (for velocity)
Range resolution	$250\,\mathrm{m}$ (for velocity)
Orientation and ellipticity	$(\pi/4, 0)$ and $(-\pi/4, 0)$

Target and receiver parameters:

- EMVS receiver located at $(3.46\,\mathrm{km}, 2\,\mathrm{km})$
- The target to be located at the origin, moving with a velocity of $30\,\mathrm{m}\,/\,\mathrm{s}$ in the positive y-axis direction

Numerical Results: Definitions

Measurement parameters:

The definitions of signal-to-noise ratio (SNR) and clutter-to-noise ratio (CNR) are given as

$$\mathrm{SNR\,(in\ dB)} = 10\log_{10}\frac{\boldsymbol{\mu}^H \boldsymbol{S}^H \boldsymbol{S}\boldsymbol{\mu}}{\sigma} \tag{32}$$

$$\mathrm{CNR\,(in\ dB)} = 10\log_{10}\frac{\mathrm{Tr}\{\boldsymbol{\Sigma}\}}{\sigma}. \tag{33}$$

The target scattering coefficients are generated from a $\mathcal{CN}(0,1)$ distribution. Similarly, the entries of the clutter covariance matrix are generated from a $\mathcal{CN}(0,1)$ distribution, and then scaled to satisfy the required SNR and CNR, respectively.

Numerical Results: Distribution of Test Statistic

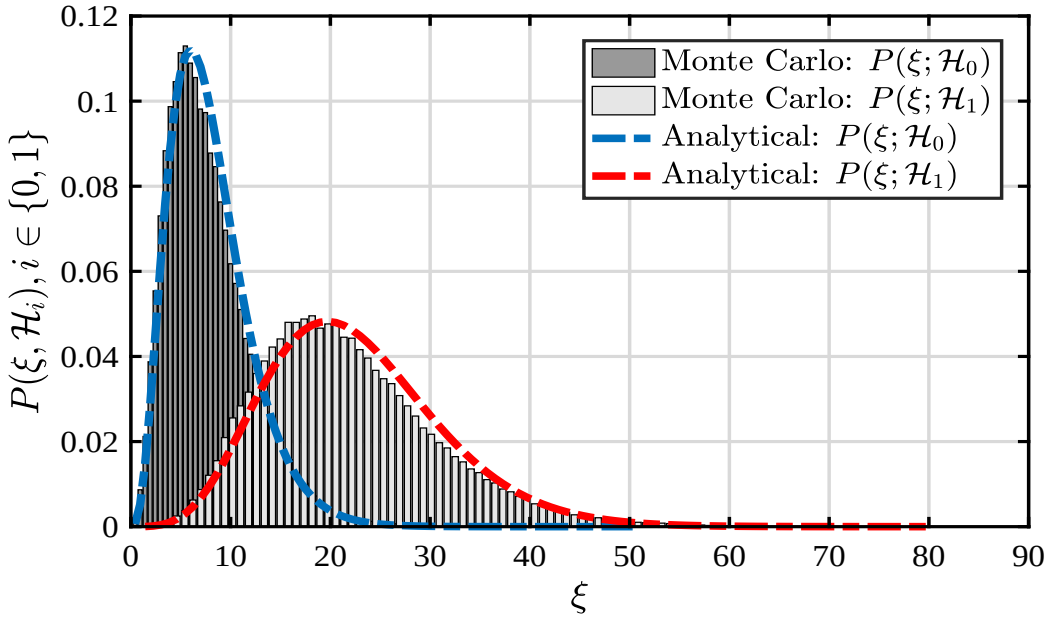

Figure 5: Normalized histogram (empirical PDF) and the analytic PDF under $\mathcal{H}_0$ and $\mathcal{H}_1$, with $\mathrm{SNR} = -10\,\mathrm{dB}$, $\mathrm{CNR} = 10\,\mathrm{dB}$, number of samples per snapshot $N = 8$, and number of snapshots $D = 200$.

Observation:

The empirical distribution closely matches the analytic distribution.

Numerical Results: Performance of the Detector

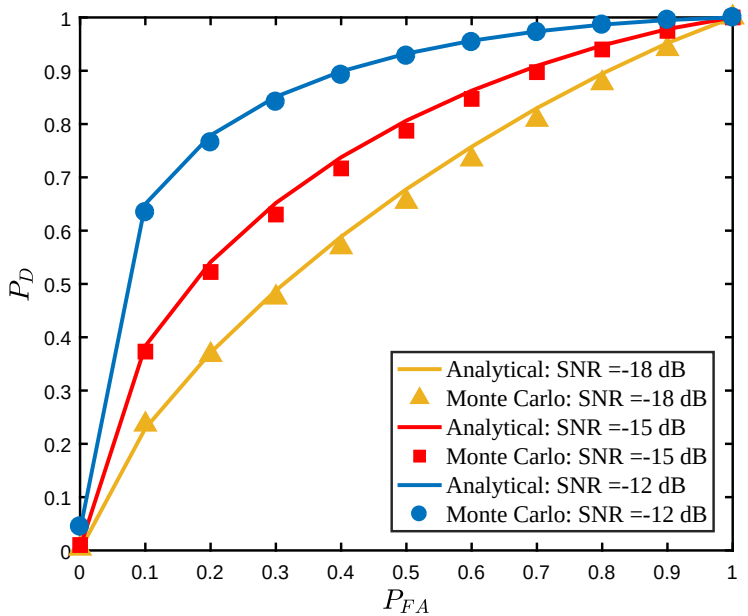

Figure 6: ROC curves for different values of SNR. The solid line plot and the scattered plot indicate the probability of detection obtained from the analytical distribution and the empirical distribution, respectively.

Observation:

The performance of the detector improves as the SNR increases.

Numerical Results: Stationary vs Moving Target

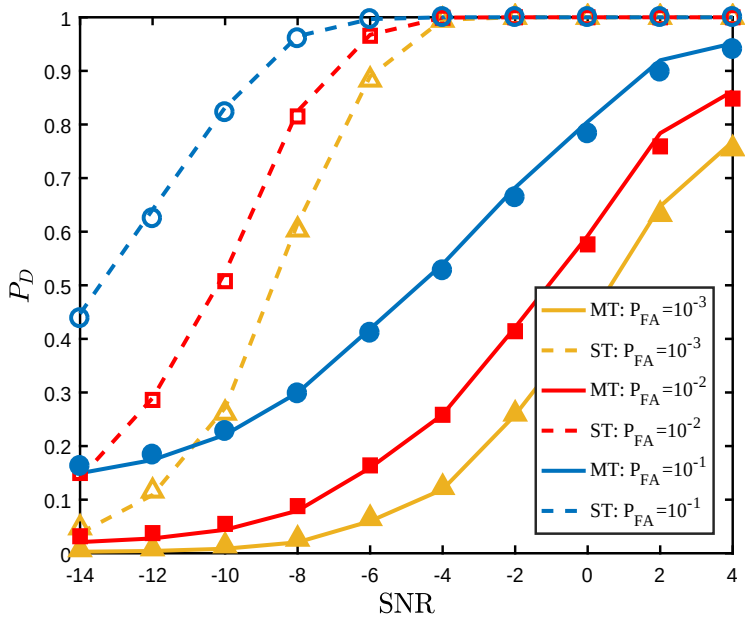

Figure 7: Probability of detection curves across different values of SNR values keeping the probability of false alarm constant. The solid line plot and the dashed line plot indicate the probability of detection obtained from the analytical distribution for a moving (MT) and a stationary target (ST), respectively. The scatter plots outlining the solid and dashed line curves indicate the probability of detection obtained from the empirical distribution for the given value of probability of false alarm.

Observation:

For a stationary target, the improvement in the performance of the detector is attributed to the fact that the inner product of the delay-Doppler matrix is $k\boldsymbol{I}_M$.

Numerical Results: SNR vs CNR

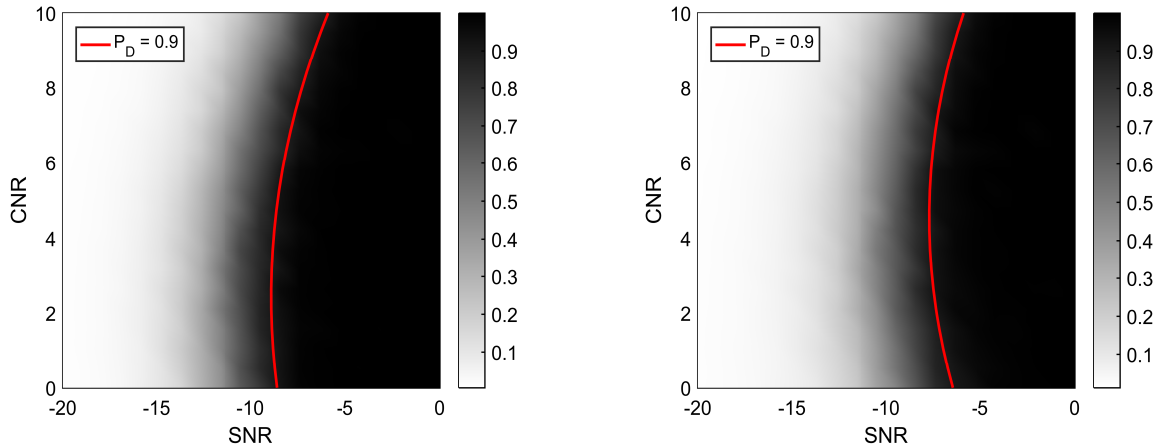

(a) Analytical distribution. **(b)** Empirical distribution.

Figure 8: Probability of detection for different values of SNR and CNR. The probability of false alarm is fixed at 10^{-3}. The number of samples per snapshot $N = 8$ and number of snapshots $D = 200$. The probability of detection is represented using gray scale pixels, where the darker pixels indicate higher values of probability of detection.

Observation:

We observe that the detector performance under both analytical and empirical distribution match closely. Further, we notice a transition phase at $\mathrm{SNR} = -10\,\mathrm{dB}$, for both analytical and empirical, probability of detection plots.

Numerical Results: Comparison with the Oracle Detector

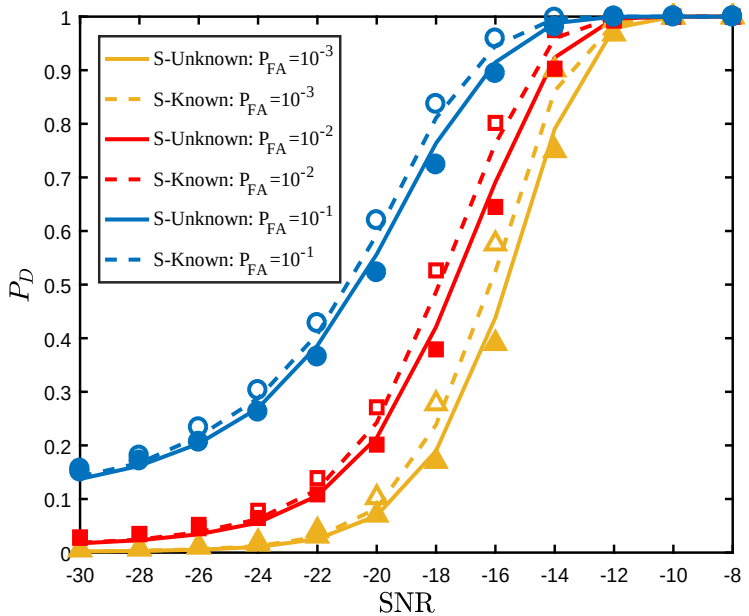

Figure 9: The solid line plot and the dashed line plot indicate the probability of detection obtained from the analytical distribution for stationary target when the signal information matrix is known and unknown, respectively. The filled and hollow marker scatter plots outlining the solid and dashed line curves indicate the probability of detection obtained from the empirical distribution for unknown and known signal information matrix, respectively.

Observation:

The proposed detector closely matches the performance of the oracle detector, however, it is important to note that the oracle detector does not require large number of snapshots.

Numerical Results: Number of Snapshots

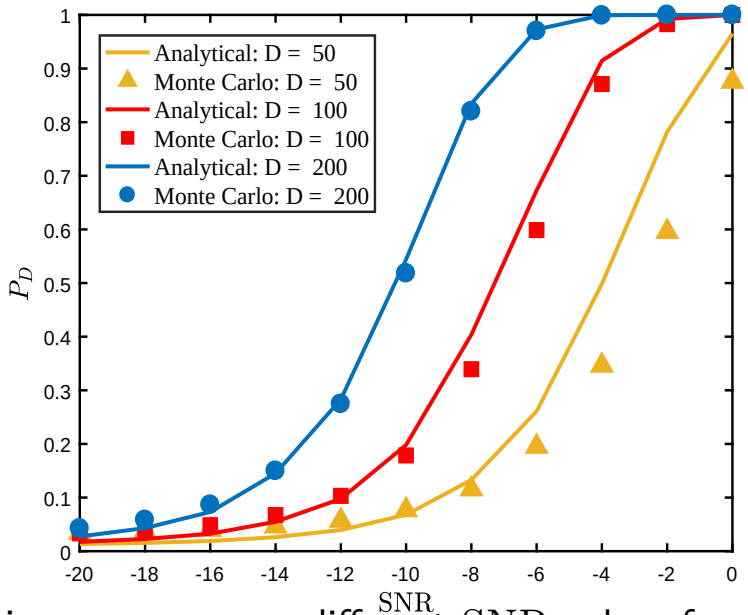

Figure 10: Probability of detection curves across different SNR values for varying number of snapshots. The solid line plot and the scattered plot indicate the probability of detection obtained from the analytical distribution and the empirical distribution, respectively. The number of samples per snapshot $N = 8$ and number of snapshots $D = \{50, 100, 200\}$, with a background $\mathrm{CNR} = 10\,\mathrm{dB}$.

Observation:

The performance of the detector improves as the number of snapshots increases. As the number of snapshots increases, the integration time to compute the probability of detection increases, thereby improving the performance of the detector.

Numerical Results: Compare Sensors

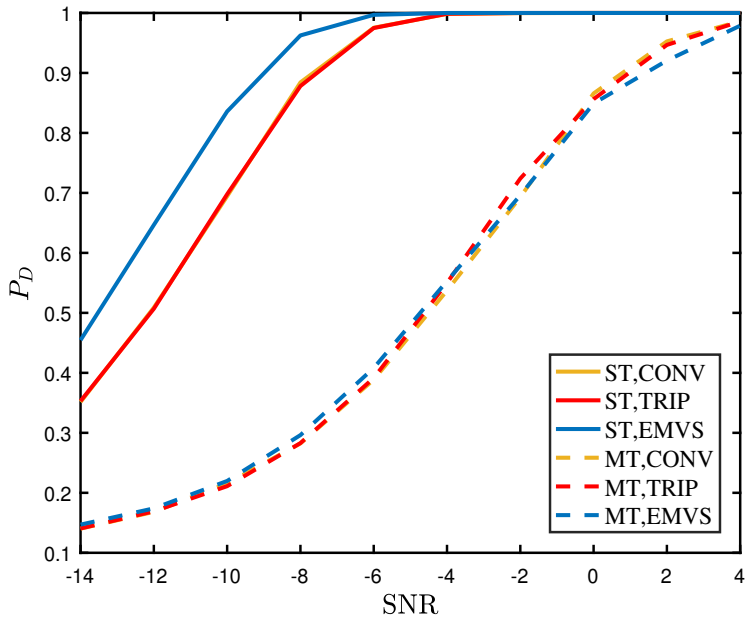

Figure 11: Probability of detection curves across different values of SNR values keeping the probability of false alarm constant. The solid line and dashed line plot indicate the probability of detection for a stationary target (ST) and a moving target (MT), respectively, for three types of sensors namely, electromagnetic vector sensors (EMVS), tripole antenna (TRIP), and conventional orthogonal antenna (CONV).

Observation:

For a moving target, the probability of detection does not vary based on the choice of the sensor because the entries of the inner product of $\boldsymbol{B}^H \boldsymbol{A}$ in the expression of the non-centrality parameter in (31) are not close to Identity matrix.

Conclusions

- Presented a GLRT-based detector for a passive radar network using EMVS, with weather radar as signal of opportunity, when the direct path signal from the transmitter is not available.
- Considered the effect of signal-dependent clutter in the surveillance channel, and derived a GLRT detector for a bistatic scenario.
- Demonstrated the CFAR property of the detector, where the expression of the test statistic under the null-hypothesis is not dependent on the transmitted signal, clutter, and noise.
- Studied the performance of the proposed detector in different bistatic scenarios, by varying the network settings such as, number of snapshots, SNR, and CNR.

Future Work

- Extend our analysis to multi-target and extended target scenario in a passive radar network.
- Consider a passive multistatic system formed by several receivers.
- Develop a centralized approach for target detection in the presence of inhomogeneous signal-dependent clutter.
- Address passive radar networks in the presence of multiple transmitters of opportunity.

Thank you!